

Floquet control of topological phases and Hall effects in Z_2 nodal line semimetals

Pu Liu,^{1,2} Chaoxi Cui,^{2,*} Lei Li,² Runze Li,² Dong-Hui Xu,^{3,4,†} and Zhi-Ming Yu^{2,5}

¹*School of Microelectronics and Physics, Hunan University of Technology and Business, Changsha 410205, China*

²*Centre for Quantum Physics, Key Laboratory of Advanced Optoelectronic Quantum Architecture and Measurement (MOE), School of Physics, Beijing Institute of Technology, Beijing, 100081, China*

³*Department of Physics, and Chongqing Key Laboratory for Strongly Coupled Physics, Chongqing University, Chongqing 400044, China*

⁴*Center of Quantum Materials and Devices, Chongqing University, Chongqing 400044, China*

⁵*International Center for Quantum Materials, Beijing Institute of Technology, Zhuhai, 519000, China*

Dynamic control of topological properties in materials is central to modern condensed matter physics, and Floquet engineering, utilizing periodic light fields, provides a promising avenue. Here, we use Floquet theory to theoretically study the topological response of a Z_2 nodal line semimetal (NLSM) when driven by circularly polarized light (CPL). We demonstrate that the direction of CPL irradiation critically dictates the resulting topological phase transitions. Specifically, when light is incident perpendicular to the nodal line plane, increasing the light amplitude induces two successive topological phase transitions: first, from the Z_2 NLSM to a vortex NLSM, a rare and intriguing topological state; and second, a transition from the vortex NLSM to a semimetal with a pair of Weyl points (WPs). In stark contrast, irradiation along other directions directly transforms the Z_2 nodal line into a pair of WPs. We further investigate the transport properties of the Floquet Z_2 NLSM, focusing on the anomalous and planar Hall effects. The anomalous Hall effect exhibits a direction-dependent amplitude variation, deviating from conventional two-band NLSM behavior. Importantly, we reveal a significant and tunable planar Hall effect, a phenomenon largely unexplored in Floquet topological materials, which is highly sensitive to both light amplitude and direction. Our findings not only present a novel route to realize the vortex NLSM, but also establish an efficient way to control Hall transport phenomena in Z_2 NLSMs.

I. INTRODUCTION

Topological semimetals (SMs) represent a novel class of quantum materials characterized by unique band structures where conduction and valence bands intersect in momentum space [1–3]. This class includes Dirac semimetals (DSMs) [4–8], Weyl semimetals (WSMs) [9–14], and nodal-line semimetals (NLSMs) [15–19], all of which have attracted significant attention in recent years due to their unique band structures and exotic quasiparticles. DSMs exist in systems preserving both time-reversal \mathcal{T} and spatial inversion \mathcal{P} symmetries, resulting in four-fold degenerate band crossings at discrete points. In contrast, WSMs require the breaking of either \mathcal{T} or \mathcal{P} symmetry, leading to pairs of Weyl points (WPs) with opposite chirality [9–13]. In contrast to DSMs or WSMs, where the conduction and valence bands intersect at discrete points in momentum space [2, 8, 9], NLSMs feature continuous lines or loops of band crossing, giving rise to distinct topological and transport phenomena [19–24].

Among NLSMs, conventional NLSMs are topologically protected by a π Berry phase and stabilized by symmetries such as \mathcal{PT} or mirror symmetries [15, 22, 23, 25]. However, theoretical advances have identified a special variant: the Z_2 NLSM [22, 26–28], distinguished by a nontrivial Z_2 monopole charge originating from the topology of real electronic states [22, 28–31]. Nodal

lines (NLs) with Z_2 monopole charges can only be created and annihilated in pairs. Z_2 NLs can appear as a consequence of double band inversion [22, 27, 28]. This distinctive band topology has been predicted in electronic band structures [27, 28, 31–33], phonon spectra [34, 35], artificial systems [36–38], and even as a photoinduced phase in Z_2 DSMs under periodic driving [39]. Additionally, another unconventional type, the vortex NLSM, has been proposed in three-dimensional systems with mirror symmetry [40, 41]. Protected by both a π Berry phase and a Z charge defined on a hemisphere enclosing the NL, vortex NLSMs are rare, with experimental realization only recently achieved in circuit metamaterials [42] and proposals in strained ZrTe and Li_2NaN [41, 43].

Floquet engineering, the use of periodic external fields such as light to dynamically manipulate material properties, has emerged as a powerful tool for tailoring topological phases of matter [44–50]. A typical example of this is the realization of the Floquet topological insulator [51–53], demonstrating the ability of periodic light fields to create nontrivial band topology. Specifically, circularly polarized light (CPL) has been predicted to induce a gap at the degenerate Dirac points of graphene, leading to a quantum Hall effect even without a magnetic field [54–56]. Periodic optical fields have also been used to generate WSMs from various parent states, including topological insulators, DSMs, and NLSMs [57–63]. Recent proposals even suggest the possibility of photoinduced higher-order topological insulators [64–67] and higher-order topological semimetals [68–71]. Beyond these topological phases, periodically driven systems can exhibit various novel transport phenomena, such as a

* cuichaoxi@bit.edu.cn

† donghuixu@cqu.edu.cn

photoinduced tunable anomalous Hall effect [72–77], as well as thermal Hall and Nernst effect [78, 79]. Notably, Floquet engineering opens avenues to generate topological states and physical properties that are absent in equilibrium conditions [67, 80–82]. In the context of NLSMs, this technique is particularly promising for tailoring their anisotropic band structures and rich topological responses.

In this work, we employ a $k \cdot p$ model combined with Floquet theory to theoretically investigate the topological transitions and transport properties of a Z_2 NLSM driven by CPL. Unlike conventional NLSMs, the Z_2 NLSM originates from a double band inversion and exhibits a unique linking structure, requiring a four-band model for its description. Consequently, the behavior of the Z_2 NL is fundamentally different from that of a normal NL. Due to the anisotropic band structure of the Z_2 NL, its response to CPL depends strongly on the light's propagation direction. Assuming the Z_2 NL resides at the $k_x=0$ plane, irradiation with the CPL along x direction induces two successive topological transitions as the light amplitude increases: first from the Z_2 NL to a vortex NL, then to a pair of WPs located on the k_x axis. The separation between these two WPs increases with increasing amplitude of light. In contrast, when the CPL is incident along the y or z direction, the Z_2 NL undergoes a direct transformation into a pair of WPs located on the k_y or k_z axis, respectively.

The presence of CPL induces a finite photo-induced anomalous Hall conductivity (AHC) in the Z_2 NLSM. At low amplitudes of light, the AHC exhibits a nonmonotonic dependence on the amplitude. However, when the amplitude of light is sufficiently strong, or the Fermi energy of the system is located near the WPs, the AHC is directly proportion to the square of the amplitude of light. We further study the planar Hall conductivity (PHC) in the driven systems, and found that the PHC can also be tuned by adjusting the direction and amplitude of the incident light. The PHC can be divided into odd J^{odd} and even components J^{even} with respect to the relaxation time. For simplicity, we focus on the scenario where external magnetic and electric fields are aligned. When the CPL is along x direction, the PHC consists only of J_x^{odd} component, remains independent of the magnetic field angle. In sharp contrast, for the system driven by CPL along the z direction, both J_z^{odd} and J_z^{even} components exhibit a periodicity of π as the direction of fields is varied.

This paper is organized as follows. In Sec. II, we derive the effective Floquet Hamiltonian of the Z_2 NLSM under off-resonant CPL using a four-band $k \cdot p$ model and Floquet theory, supplemented by two-band models near the Γ point and the photo-induced WPs. In Secs. III and IV, we respectively study the AHC and PHC under the irradiation of CPL in different directions. Conclusions are given in Sec. V.

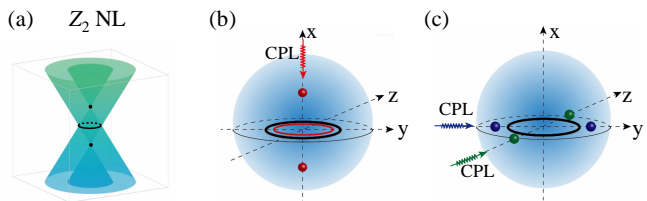


FIG. 1. (a) A Z_2 NL has band-touching rings on the $k_x=0$ plane. (b) Schematic diagram of topological phase transitions for Z_2 NL driven by CPL in x direction. The red ring (denoting vortex NL) and dots (denoting WPs) represent the case for the amplitude of light $A < A_c$ and $A > A_c$, respectively. (c) Schematic diagram of topological phase transitions of Z_2 NL driven by CPL in y and z direction, which represent by the blue and green dots (denoting WPs), respectively. The black rings in (b-c) denote the original Z_2 NL without CPL.

II. FLOQUET HAMILTONIAN OF THE PERIODICALLY DRIVEN Z_2 NLSM

A. General description

Z_2 NLSM that arises from a double band inversion is generally described by a four-band model [22, 28],

$$H_0(\mathbf{k}) = k_x \sigma_x + k_y \tau_y \sigma_y + k_z \sigma_z + m \tau_z \sigma_z, \quad (1)$$

where $\tau_{x,y,z}$ and $\sigma_{x,y,z}$ are Pauli matrices acting on two isospin degrees. The energy dispersion of the system is

$$\varepsilon(\mathbf{k}) = \pm \sqrt{k_x^2 + (k_{||} \pm m)^2}, \quad (2)$$

where $k_{||} = \sqrt{k_y^2 + k_z^2}$. For half filling, the conduction and valence bands cross and form a closed loop, which is located on the $k_x=0$ plane with a radius of $|m|$. Besides, the two occupied bands cross along another line $k_{||}=0$, which is linked with the Z_2 NL. The schematic band structure of this model is shown in Fig. 1(a), with Z_2 NL plotted by the black ring and the other band degeneracy points represented by black dots.

To explore the impact of periodic driving on the band structure and topological response of the Z_2 NLSM, we subject the system to a periodic CPL applied in three different directions. The period of CPL is $T = \frac{2\pi}{\omega}$ with ω being the frequency of light. The intensity of CPL can be expressed as $\mathcal{E}(\tau) = -\partial_\tau \mathbf{A}(\tau)$ with a time periodic vector potential $\mathbf{A}(\tau) = \mathbf{A}(\tau+T)$. The Hamiltonian and eigenstates of the driven system become periodic and fulfils $H(\tau) = H(\tau+T)$, and $|\Phi(\tau)\rangle = |\Phi(\tau+T)\rangle$. Floquet theory simplifies the solution of the Schrödinger equation for a time periodic Hamiltonian to an eigenvalue problem for a time-independent [44, 45]. Using the Fourier transformation $H(\tau) = \sum_n e^{-in\omega\tau} H_n$ and $|\Phi(\tau)\rangle = \sum_n e^{-in\omega\tau} |\Phi^n\rangle$, the time-dependent Schrödinger equation

tion is mapped to a static eigenvalues problem [83, 84],

$$\sum_n (H_{m-n} - n\omega\delta_{mn})|\Phi_\alpha^n\rangle = \epsilon_\alpha|\Phi_\alpha^n\rangle, \quad (3)$$

in the extended Floquet space. Here, we are concerned with the high-frequency light, whose frequency is much larger than the energy scales of the system. According to the Magnus expansion, the effective Floquet Hamiltonian up to $1/\omega$ can be expanded as [54–56]

$$H_{\text{eff}} = H_0 + \frac{[H_{-1}, H_1]}{\omega}, \quad (4)$$

where the higher-order terms of $1/\omega$ is dropped. Due to the anisotropic band structure of the Z_2 NL, we investigate its topological phase transitions under driving by the CPL along different directions.

B. CPL along x direction

We first study the system driven by CPL along x direction, with vector potential $\mathbf{A} = A(0, \eta \sin \omega\tau, \cos \omega\tau)$. Since amplitude of light $A = e\mathcal{E}\omega^{-1}$ with \mathcal{E} denoting field strength, it is adjustable in the experiment by simply tuning \mathcal{E} . $\eta = 1$ and $\eta = -1$ represent the right- and left-handed CPL, respectively. Following the standard approach, the electromagnetic coupling is given by $H(\mathbf{k}) \rightarrow H[\mathbf{k} - e\mathbf{A}(\tau)]$. In this case, the effective Floquet $k \cdot p$ Hamiltonian in the high frequency limit becomes

$$H_{\text{eff}}^x = H_0 - \frac{1}{2\omega} i\eta A^2 [\sigma_z, \tau_y \sigma_y]. \quad (5)$$

Compared to undriven system Eq. (1), the Hamiltonian gains an additional correction term. Although the \mathcal{T} symmetry of the driven system is broken by CPL, it still has $\mathcal{C}_{2y(2z)}\mathcal{T}$ symmetry. The eigenvalues for the driven system is obtained as

$$\epsilon = \pm \sqrt{k_{\parallel}^2 + k_x^2 + m^2 + \frac{A^4}{\omega^2} \pm 2\sqrt{m^2 k_{\parallel}^2 + \frac{A^4}{\omega^2} (k_x^2 + m^2)}}. \quad (6)$$

The evolution of band structures with increasing A is schematically depicted in Fig. 1(b). The black ring on the $k_x=0$ plane represents the Z_2 NL for the original system. As A increases, the driven system undergoes two topological phase transitions. In the regime of low light amplitude, specifically when $A < A_c$ ($A_c = \sqrt{m\omega}$), the radius of the NL located on the $k_x=0$ plane continuously decreases as A increases, which is plotted as the red ring in Fig. 1(b). Simultaneously, the degeneracy between the two occupied states is lifted, breaking the linking structure of the Z_2 NL [see Fig. 2(a)]. Intriguingly, the resulting NL is not a conventional NL but a vortex NL. To directly demonstrate it, we derive a two-band effective

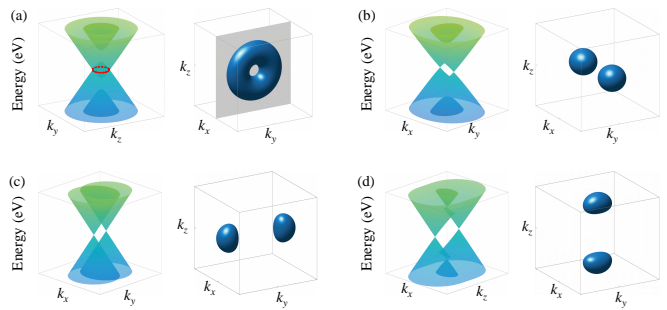


FIG. 2. The band structures and Fermi surfaces for $E_F = 0.05$ eV for Z_2 NL driven by CPL. The CPL is along x direction with amplitudes of light (a) $A=0.5 \text{ \AA}^{-1} < A_c$, and (b) $A=1 \text{ \AA}^{-1} > A_c$. The CPL is along (c) y direction and (d) z direction with $A=1 \text{ \AA}^{-1}$. We take the other model parameters as $m=0.1$ eV and $\omega=6$ eV.

model from Eq. (5) to describe the low-energy bands, expressed as

$$H_{vNL} = \frac{1}{m + \frac{A^2}{\omega}} [(k_x^2 - k_y^2 - k_z^2 + m^2 - 4\frac{A^4}{\omega^2})\sigma_z + 2k_x k_y \sigma_x + 2i k_x k_z \sigma_y]. \quad (7)$$

Using the two-band model, we plotted the band structure (red dashed line) near the Γ point in Fig. 3(a) and compared it with the result calculated from Eq. 5 (black solid line). This comparison validates the accuracy of our effective two-band description near the zone center. To further characterize the topological nature of the resulting NL, we calculated the winding number of both upper ($k_x > 0$ region) and lower ($k_x < 0$ region) hemispheres on each side of the NL [40]. These calculations yielded winding numbers of $w = +1$ and $w = -1$, respectively. This is distinct from the normal NL and the Z_2 NL, both of which exhibit a winding number of $w = 0$. The presence of non-zero and opposite winding numbers classifies this specific type of NL as a vortex [40, 41]. Therefore, our findings indicate that under driving of CPL in x direction with an amplitude below a critical value $A < A_c$, the Z_2 NL undergoes a transition to a vortex NL, thus presenting a potentially straightforward method for the experimental realization of this intriguing topological state.

At the critical point $A = A_c$, the vortex NL on the $k_x = 0$ plane shrinks into a point. Further increasing A , a pair of WPs appear, residing on the k_x axis, as shown in the Fig. 1(b) and Fig. 2(b). The locations of the WPs are tunable by changing amplitude and frequency of CPL, which is $\mathbf{k}_{w,x}^\pm = \pm(\sqrt{\frac{A^4}{\omega^2} - m^2}, 0, 0)$. We also establish an effective Hamiltonian to investigate the topological properties of these WPs. Up to the linear term, the effective two-band Hamiltonian is obtained as

$$H_{\pm}^x = -\sqrt{\frac{A^4 - \omega^2 m^2}{A^4}} (\mp q_x \sigma_z + q_z \sigma_x + q_y \sigma_y), \quad (8)$$

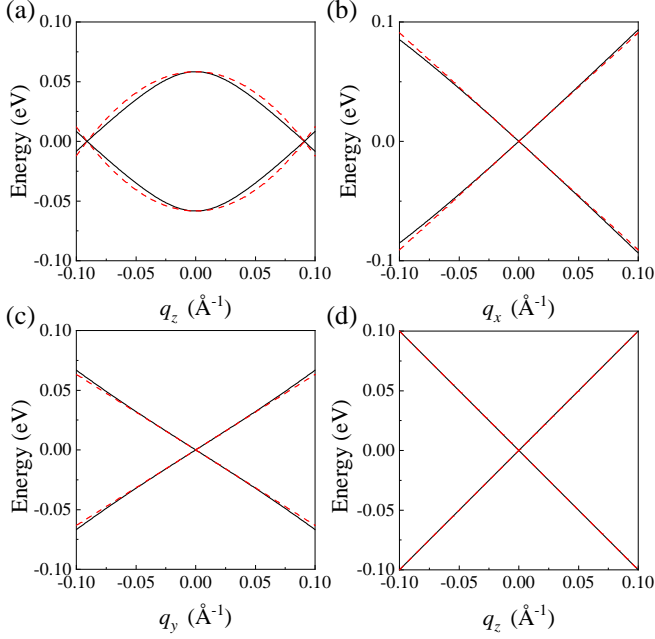


FIG. 3. The band structure for driven systems around Γ and WP. (a-b) The CPL is along x direction with amplitudes of light $A=0.5 \text{ \AA}^{-1}$ and $A=1.2 \text{ \AA}^{-1}$, respectively. (c-d) The CPL is along z direction with amplitude of light $A=0.7 \text{ \AA}^{-1}$. The band plotted by the black line are calculated by the Eq. 5 and Eq. 9, which plotted by the red dashed line are calculated by the two band model Eq. 7, Eq. 8 and Eq. 12. We take the model parameters as $m=0.1 \text{ eV}$ and $\omega=6 \text{ eV}$.

where the momentum \mathbf{q} is measured from $\pm(\sqrt{\frac{A^4}{\omega^2} - m^2}, 0, 0)$. The band structure near a WP at $\mathbf{k}_{w,x}^+$ with $A = 1.2 \text{ \AA}^{-1}$ is shown in Fig. 3(b), where the red dashed lines are calculated by the Eq. (8), and the black solid lines are calculated by Eq. (5). One observes that the band structures are almost the same around the WP. Furthermore, we calculate the winding number (Chern number) of the WP via the effective Hamiltonian (8), and find that the two WPs at $\mathbf{k}_{w,x}^\pm$ have opposite winding number of $w = \pm 1$.

C. CPL along z direction

When the propagation direction of CPL is along the z direction $\mathbf{A} = A(\eta \sin \omega\tau, \cos \omega\tau, 0)$, the effective Floquet Hamiltonian is established as

$$H_{\text{eff}}^z = H_0 - \frac{1}{2\omega} i\eta A^2 [\sigma_x, \tau_y \sigma_y], \quad (9)$$

for which the eigenvalue is

$$\epsilon = \pm \sqrt{k_{\parallel}^2 + k_x^2 + m^2 + \frac{A^4}{\omega^2} \pm 2\sqrt{m^2 k_{\parallel}^2 + \frac{A^4}{\omega^2} k_z^2}}. \quad (10)$$

When CPL is incident along the z direction, the Z_2 NL will directly transform into a pair of WPs along the z axis located at $\mathbf{k}_{w,z}^\pm = (0, 0, \pm\sqrt{\frac{A^4}{\omega^2} + m^2})$, as illustrated in Fig. 1(c).

Similarly, if CPL is along the y direction, the Floquet Hamiltonian becomes

$$H_{\text{eff}}^y = H_0 - \frac{1}{2\omega} i\eta A^2 [\sigma_x, \sigma_z], \quad (11)$$

where two WPs located at $(0, \pm\sqrt{\frac{A^4}{\omega^2} + m^2}, 0)$ appear [see the blue dots in Fig. 1(c)]. The locations for the WPs can also be adjusted by amplitude and frequency of CPL. Moreover, as shown in Fig. 2(c-d), the band structures of the system driven by CPL in y or z direction are similar. Therefore, in subsequent calculations, we only show the result for the system driven by CPL in z direction.

We also obtained a two-band model to describe the WPs located on k_z axis, expressed as

$$H_{\pm}^z = q_z \sigma_z + q_x \sigma_x \pm \sqrt{\frac{A^4}{m^2 \omega^2 + A^4} q_y \sigma_y}, \quad (12)$$

where the momentum \mathbf{q} is measured from $(0, 0, \pm\sqrt{\frac{A^4}{\omega^2} + m^2})$. Using the two-band model, we have also plotted the band structure along the q_y and q_z directions around the WP at $\mathbf{k}_{w,z}^+$ for $A = 0.7 \text{ \AA}^{-1}$, as shown in Fig. 3(c-d). Regardless of the magnitude of A , the band structure along q_z direction always remains linear, while it along the q_y directions is effected by non-linear terms when A is small. However, we have checked that this effect diminishes as A increases. Consequently, when A is large, the photo-induced WPs become an ideal linear WP.

The Z_2 NL, as a distinctive topological structure within condensed matter systems, offers an appealing platform to explore novel physical properties. In the following, based on the effective Hamiltonian derived in this section and Boltzmann transport theory, we will explore the anomalous Hall effect and planar Hall effect for the Z_2 NL driven by the CPL in different directions. Through this comprehensive analysis, we aim to deepen our understanding of topological phase transitions for Z_2 NL under light field manipulation and their potential applications in quantum materials.

III. ANOMALOUS HALL EFFECT

Under the driving of CPL, one of the significant consequences of topological transition is the emergence of the anomalous Hall effect characterized by a non-zero AHC. The CPL breaks the \mathcal{T} symmetry and leads to a photo-induced anomalous Hall effect, which can be adjusted by amplitude and frequency of CPL [54, 72, 77]. Using linear response theory, the AHC can be obtained as [54]

$$\sigma_{\mu\nu}^{\text{AHE}} = e^2 \int \frac{d\mathbf{k}}{(2\pi)^3} \sum_n f_n^0(k) \Omega_k^\rho, \quad (13)$$

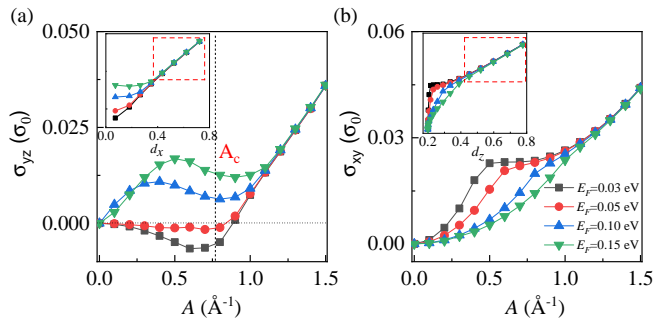


FIG. 4. The dependence of AHC on the amplitude for the system driven by the CPL in the (a) x and (b) z direction. The common parameters in use are $m = 0.1$ eV, $B = 0.5$ T, $\omega = 6$ eV, and we have defined the shorthand notation $\sigma_0 = \frac{e^2}{h}$. The variation of AHC with the distance between the two WPs is shown in the inset of the figures.

where $\mu, \nu, \rho=x, y, z$, and n is the band index. Ω_k^ρ is the Berry curvature and $f_n^0(k)$ is the occupation function. The AHC depends not only on the Berry curvature but also on the fermion occupation. In Fig. 4, we show the variation of AHC with amplitudes of light when the CPL is along x and z directions.

The topological phase transitions induced by CPL along different directions result in distinct characteristics of AHC. When the CPL is along x direction, the dependence of σ_{yz}^{AHE} on amplitude A for different Fermi levels are shown in Fig. 4(a). As aforementioned, the system driven by the CPL in x direction undergoes two topological phase transitions as amplitude increases. Correspondingly, the characteristics of the AHE are completely different in the two stages. Initially, the Z_2 NL transforms into a vortex NL with $A < A_c$, in such case the system features a torus-shape Fermi surface when the Fermi energy is small. However, when the Fermi energy is large, the Fermi surface is ellipsoid. Therefore, for $A < A_c$, the variation of σ_{yz}^{AHE} at lower Fermi energy are different from that at higher Fermi energy [see Fig. 4(a)].

In contrast, when the amplitude of light becomes large, the AHC feature a universal behavior regardless of the Fermi energy, as shown in Fig. 4(a). For $A > A_c$, the driven system undergoes the second topological phase transition, transforming into a pair of WPs. The distance between the two WPs is $d_x = 2\sqrt{\frac{A^4}{\omega^2} - m^2}$. When A is relatively large, as indicated by the dashed box in the inset in Fig. 4(a), the distance between the two WPs increases with the increases of A , which differs from the WPs generated by driving a normal NL with a large A . [72, 77].

For a Weyl semimetal with two well separated WPs, the AHC is proportional to the distance between the two WPs [12]. Therefore, as illustrated in the inset of Fig. 4(a), when $A > A_c$, the σ_{yz}^{AHE} indeed increases linearly with the distance d_x when A is large enough or the Fermi energy is small. Furthermore, since the distance

d_x is mainly controlled by the amplitude A and increases from zeros, it can be expanded as $d_x \propto (A - A_c)^{1/2}$ around the critical point A_c . This means that for $E_F=0$ and $T=0$, the AHC σ_{yz}^{AHE} is approximately proportional to the $(A - A_c)^{1/2}$ around the critical point A_c . However, for non-zero Fermi levels, a larger amplitude is required to transform the Fermi surface into a pair of separated spheres. Therefore, for a larger Fermi energy, a larger A is needed to observe the proportional relationship between AHE and d_x [see the inset in Fig. 4(a)].

Then, we discuss the AHC of the Z_2 NL under the driving of CPL in z direction, in such case, the system directly transitions into Weyl semimetal with a pair of WPs at the k_z axial. The distance between the two WPs is $d_z = 2\sqrt{\frac{A^4}{\omega^2} + m^2}$, which also increases from $|m|$ with increasing of A . However when A is small, the AHC is not proportional to d_z even for the case of $E_F=0$ and $T=0$, as AHC of the original Z_2 NL ($A = 0$) is zero. Therefore, the AHC show a nonanalytical behavior for small A , as shown in Fig. 4(b). When A is large enough, a linear relationship between σ_{xy}^{AHE} and d_z appears [see Fig. 4(b)]. Further, regardless of the direction of the incident light, the AHC of the Floquet Z_2 NL is always proportional to the distance between the two WPs when A is large.

IV. PLANER HALL EFFECT

We then study the planar Hall effect for the Z_2 NL driven by the CPL based on the semiclassical Boltzmann transport theory [85, 86]. Keeping only the linear order of electric field \mathbf{E} and magnetic field \mathbf{B} , the PHC based on the parity of time can be divided into two parts [86],

$$\mathbf{J} = \mathbf{J}^{\text{odd}} + \mathbf{J}^{\text{even}}, \quad (14)$$

$$\begin{aligned} \mathbf{J}_\mu^{\text{even}} &= e^3 \tau^2 \int [d\mathbf{k}] v_\mu [(\mathbf{v} \times \mathbf{B}) \cdot \partial_{\mathbf{k}} (\mathbf{v} \cdot \mathbf{E})] \partial_\epsilon f_k^0, \\ \mathbf{J}_\mu^{\text{odd}} &= -e^3 \tau \int [d\mathbf{k}] v_\mu (\mathbf{v} \cdot \mathbf{E}) (\mathbf{B} \cdot \boldsymbol{\Omega}_{\mathbf{k}}) \partial_\epsilon f_k^0 \\ &\quad - \frac{e^2}{\hbar} \tau \int [d\mathbf{k}] [v_\mu \partial_{\mathbf{k}} (\mathbf{m} \cdot \mathbf{B}) \cdot \mathbf{E} + \partial_{k_\mu} (\mathbf{m} \cdot \mathbf{B}) (\mathbf{v} \cdot \mathbf{E})] \partial_\epsilon f_k^0 \\ &\quad + e^3 \tau \int [d\mathbf{k}] [B_\mu (\mathbf{v} \cdot \mathbf{E}) + v_\mu (\mathbf{B} \cdot \mathbf{E})] (\mathbf{v} \cdot \boldsymbol{\Omega}_{\mathbf{k}}) \partial_\epsilon f_k^0 \end{aligned}$$

where $\mu = x, y, z$ is the direction, $v_\mu = \partial \epsilon(\mathbf{k})/\hbar$ is the velocity of electrons, and \mathbf{m} is the orbit magnetic moment. For specifically, in subsequent calculations, we focus on the case that $\mathbf{E} \parallel \mathbf{B}$, and the both fields are perpendicular to the direction of light. Due to anisotropic band structure, the PHC of the Floquet Z_2 NL also has strongly dependence on the direction of the incident light.

We first investigated the PHC of the system with CPL along x direction. In this case, \mathbf{E} and \mathbf{B} are confined in the y - z plane, i.e. $\mathbf{B} = B(0, \cos \theta, \sin \theta)$ and

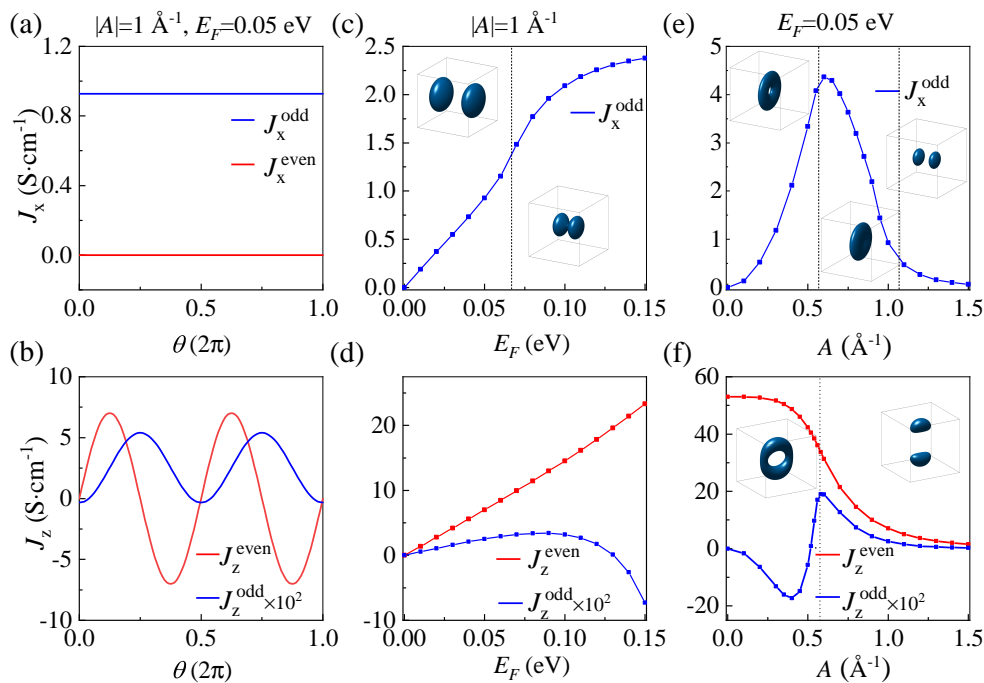


FIG. 5. The PHC versus (a-b) θ , (c-d) Fermi level E_F and (e-f) the amplitudes of CPL. The incident light is along the (a) (c) (e) x direction and (b)(d)(f) z direction, respectively. The common parameters in use are $m = 0.1$ eV, $B = 0.5$ T and $\omega = 6$ eV.

$\mathbf{E} = E(0, \cos \theta, \sin \theta)$. From Hamiltonian (5), one observes that while the \mathcal{T} symmetry is broken by CPL, the system still keeps $\mathcal{C}_{2y}\mathcal{T} = \tau_0\sigma_z\mathcal{K}$ symmetry. This means that the PHC J_x would only have the term of J_x^{odd} , as J_x^{even} is forbidden by $\mathcal{C}_{2y}\mathcal{T}$. In Fig. 5(a), we plot the variation of J_x with θ , when the amplitude is $A=1 \text{ \AA}^{-1}$ and Fermi level is $E_F=0.05$ eV, where the Z_2 NL has already transitioned into a pair of WPs, and the corresponding Fermi surface consists of two spheres. From Fig. 5(a), we indeed have $J_x^{\text{even}} = 0$ regardless of the value of θ , and J_x^{odd} is finite. Interestingly, J_x^{odd} also does not depend on θ , as the effective Hamiltonian (5) is isotropic in the k_y - k_z planes.

The dependence of the PHC on Fermi level E_F with fixed A ($A=1 \text{ \AA}^{-1}$) and θ ($\theta = 0^\circ$) is shown in Fig. 5(c). When E_F is small, the Fermi surface consists of two separate spheres, and J_x^{odd} approximately linearly increases with E_F . At a critical point E_F^c , a Lifshitz phase transition happens and the two separated Fermi spheres merge into a single one [see Fig. 5(c)]. For $E_F > E_F^c$, while the PHC J_x^{odd} still increases with E_F , but gradually deflects from linear increase. In contrast, for $E_F = 0.05$ eV, when the amplitude increases, the Fermi surface of the system evolves from a torus-shape to a closed surface and eventually transforms into a pair of spheres. This makes the variation of the J_x^{odd} on A not a monotone increasing function, which increases at first and then decreases, as shown in Fig. 5(e).

Then, we consider the case that the CPL is along the z direction, and the \mathbf{E} and \mathbf{B} are confined in the x - y plane,

i.e. $\mathbf{E} = E(\cos \theta, \sin \theta, 0)$ and $\mathbf{B} = B(\cos \theta, \sin \theta, 0)$. In Fig. 5(b), we plot the J_z as a function of θ . We find that both J_z^{even} and J_z^{odd} are finite, and have a period of π owing to the setup of $\mathbf{E} \parallel \mathbf{B}$. For $\theta = \pi/4$, we calculate the PHC as a function of E_F and A . When the Fermi level is small, both J_z^{even} and J_z^{odd} almost linearly increase with E_F [see Fig. 5(d)]. However, when E_F is large, an opposite trend in the variation of J_z^{even} and J_z^{odd} is observed. For $E_F = 0.05$ eV, as A increases, we find that J_z^{even} monotonically decreases, while J_z^{odd} feature a complicated behavior, as shown in Fig. 5(f).

V. SUMMARY

In this work, based on the $k \cdot p$ model and Floquet theory, we study the topological phase transition, the anomalous and planar Hall effects of the Z_2 NL driven by the CPL in different directions. When the incident CPL is along x direction, the system undergoes two topological phase transitions: from the Z_2 NL to vortex NL and then to a pair of WPs. This provides a convenient method for obtaining vortex NL. However, when the CPL is along the y or z direction, the system will directly transition into a pair of WPs located on the k_y or k_z axis. Moreover, as the amplitude of light increases, the distance between the two photo-induced WPs continuously increases, which makes the AHC of the driven Z_2 NL increases with the amplitude of light. Besides, the PHC of the Floquet Z_2 NL can also be modulated by the direc-

tion and amplitude of the incident light. These findings deepen our understanding of the Floquet engineering on the Z_2 NL, offer different methods to realize vortex NL, and may be useful for designing novel AHC and PHC devices.

ACKNOWLEDGMENTS

This work was supported by the National Natural Science Foundation of China (Grant Nos. 12474040,

12474151, and 12347101), the Natural Science Foundation of Chongqing (Grant No. CSTB2022NSCQ-MSX0568) and Beijing National Laboratory for Condensed Matter Physics (No. 2024BNLCMPKF025).

-
- [1] A. A. Burkov, Topological semimetals, *Nat. Mater.* **15**, 1145 (2016).
- [2] N. Armitage, E. Mele, and A. Vishwanath, Weyl and Dirac semimetals in three-dimensional solids, *Rev. Mod. Phys.* **90**, 015001 (2018).
- [3] Z.-M. Yu, Z. Zhang, G.-B. Liu, W. Wu, X.-P. Li, R.-W. Zhang, S. A. Yang, and Y. Yao, Encyclopedia of emergent particles in three-dimensional crystals, *Sci. Bull.* **64**, 375 (2022).
- [4] Z. Wang, Y. Sun, X.-Q. Chen, C. Franchini, G. Xu, H. Weng, X. Dai, and Z. Fang, Dirac semimetal and topological phase transitions in $A_3\text{Bi}$ ($A = \text{Na}, \text{K}, \text{Rb}$), *Phys. Rev. B* **85**, 195320 (2012).
- [5] Z. Wang, H. Weng, Q. Wu, X. Dai, and Z. Fang, Three-dimensional Dirac semimetal and quantum transport in Cd_3As_2 , *Phys. Rev. B* **88**, 125427 (2013).
- [6] M. Neupane, S.-Y. Xu, R. Sankar, N. Alidoust, G. Bian, C. Liu, I. Belopolski, T.-R. Chang, H.-T. Jeng, H. Lin, A. Bansil, F. Chou, and M. Z. Hasan, Observation of a three-dimensional topological Dirac semimetal phase in high-mobility Cd_3As_2 , *Nat. Commun.* **5**, 3786 (2014).
- [7] Z. K. Liu, J. Jiang, B. Zhou, Z. J. Wang, Y. Zhang, H. M. Weng, D. Prabhakaran, S.-K. Mo, H. Peng, P. Dudin, T. Kim, M. Hoesch, Z. Fang, X. Dai, Z. X. Shen, Z. H. D. L. Feng, and Y. L. Chen, A stable three-dimensional topological Dirac semimetal Cd_3As_2 , *Nat. Mater.* **13**, 577 (2014).
- [8] S. M. Young, S. Zaheer, J. C. Y. Teo, C. L. Kane, E. J. Mele, and A. M. Rappe, Dirac Semimetal in Three Dimensions, *Phys. Rev. Lett.* **108**, 140405 (2012).
- [9] X. Wan, A. M. Turner, A. Vishwanath, and S. Y. Savrasov, Topological semimetal and Fermi-arc surface states in the electronic structure of pyrochlore iridates, *Phys. Rev. B* **83**, 205101 (2011).
- [10] B. Q. Lv, H. M. Weng, B. B. Fu, X. P. Wang, H. Miao, J. Ma, P. Richard, X. C. Huang, L. X. Zhao, G. F. Chen, Z. Fang, X. Dai, T. Qian, and H. Ding, Experimental Discovery of Weyl Semimetal TaAs, *Phys. Rev. X* **5**, 031013 (2015).
- [11] B. Q. Lv, N. Xu, H. M. Weng, J. Z. Ma, P. Richard, X. C. Huang, L. X. Zhao, G. F. Chen, C. E. Matt, F. Bisti, V. N. Strocov, J. Mesot, Z. Fang, X. Dai, T. Qian, M. Shi, and H. Ding, Observation of Weyl nodes in TaAs, *Nat. Phys.* **11**, 724 (2015).
- [12] A. A. Burkov and L. Balents, Weyl Semimetal in a Topological Insulator Multilayer, *Phys. Rev. Lett.* **107**, 127205 (2011).
- [13] K.-Y. Yang, Y.-M. Lu, and Y. Ran, Quantum Hall effects in a Weyl semimetal: Possible application in pyrochlore iridates, *Phys. Rev. B* **84**, 075129 (2011).
- [14] H. Weng, C. Fang, Z. Fang, B. A. Bernevig, and X. Dai, Weyl Semimetal Phase in Noncentrosymmetric Transition-Metal Monophosphides, *Phys. Rev. X* **5**, 011029 (2015).
- [15] Y.-H. Chan, C.-K. Chiu, M. Y. Chou, and A. P. Schnyder, Ca_3P_2 and other topological semimetals with line nodes and drumhead surface states, *Phys. Rev. B* **93**, 205132 (2016).
- [16] C. Fang, L. Lu, J. Liu, and L. Fu, Topological semimetals with helicoid surface states, *Nat. Phys.* **12**, 936 (2016).
- [17] Y. Chen, Y. Xie, S. A. Yang, H. Pan, F. Zhang, M. L. Cohen, and S. Zhang, Nanostructured Carbon Allotropes with Weyl-like Loops and Points, *Nano Lett.* **10**, 6974 (2015).
- [18] T. Bzdušek, Q. Wu, A. Rüegg, M. Sgrist, and A. A. Soluyanov, Nodal-chain metals, *Nature* **538**, 75 (2016).
- [19] A. A. Burkov, M. D. Hook, and L. Balents, Topological nodal semimetals, *Phys. Rev. B* **84**, 235126 (2011).
- [20] H. Weng, Y. Liang, Q. Xu, R. Yu, Z. Fang, X. Dai, and Y. Kawazoe, Topological node-line semimetal in three-dimensional graphene networks, *Phys. Rev. B* **92**, 045108 (2015).
- [21] X. Zhang, Z.-M. Yu, Y. Lu, X.-L. Sheng, H. Y. Yang, and S. A. Yang, Hybrid nodal loop metal: Unconventional magnetoresistance and material realization, *Phys. Rev. B* **97**, 125143 (2018).
- [22] C. Fang, Y. Chen, H.-Y. Kee, and L. Fu, Topological nodal line semimetals with and without spin-orbital coupling, *Phys. Rev. B* **92**, 081201(R) (2015).
- [23] C.-K. Chiu and A. P. Schnyder, Classification of reflection-symmetry-protected topological semimetals and nodal superconductors, *Phys. Rev. B* **90**, 205136 (2014).
- [24] Y. Kim, B. J. Wieder, C. L. Kane, and A. M. Rappe, Dirac Line Nodes in Inversion-Symmetric Crystals, *Phys. Rev. Lett.* **115**, 036806 (2015).
- [25] Y. X. Zhao, A. P. Schnyder, and Z. D. Wang, Unified Theory of PT and CP Invariant Topological Metals and Nodal Superconductors, *Phys. Rev. Lett.* **116**, 156402 (2016).
- [26] Z. Song, T. Zhang, and C. Fang, Diagnosis for Nonmagnetic Topological Semimetals in the Absence of Spin-Orbital Coupling, *Phys. Rev. X* **8**, 031069 (2018).

- [27] T. Kawakami, T. Nomura, and M. Koshino, Electronic properties of a graphyne- N monolayer and its multilayer: Even-odd effect and topological nodal line semimetallic phases, *Phys. Rev. B* **102**, 115421 (2020).
- [28] J. Ahn, D. Kim, Y. Kim, and B.-J. Yang, Band Topology and Linking Structure of Nodal Line Semimetals with Z_2 Monopole Charges, *Phys. Rev. Lett.* **121**, 106403 (2018).
- [29] T. Morimoto and A. Furusaki, Weyl and Dirac semimetals with Z_2 topological charge, *Phys. Rev. B* **89**, 235127 (2014).
- [30] Y. X. Zhao and Y. Lu, PT -Symmetric Real Dirac Fermions and Semimetals, *Phys. Rev. Lett.* **118**, 056401 (2017).
- [31] C. Chen, X.-T. Zeng, Z. Chen, Y. X. Zhao, X.-L. Sheng, and S. A. Yang, Second-Order Real Nodal-Line Semimetal in Three-Dimensional Graphdiyne, *Phys. Rev. Lett.* **128**, 026405 (2022).
- [32] X. Gao, Y. Zhu, D. Yi, J. Zhou, S. Zhang, C. Yin, F. Ding, S. Zhang, X. Yi, J. Wang, L. Tong, Y. Han, Z. Liu, and J. Zhang, Ultrathin graphdiyne film on graphene through solution-phase van der Waals epitaxy, *Sci. Adv.* **4**, eaat6378 (2018).
- [33] T. Nomura, T. Habe, R. Sakamoto, and M. Koshino, Three-dimensional graphdiyne as a topological nodal-line semimetal, *Phys. Rev. Mater.* **2**, 054204 (2018).
- [34] Y. Han, Y. Liu, C. Cui, C.-C. Liu, and Z.-M. Yu, Crossed real nodal-line phonons in gold monobromide, *Phys. Rev. B* **110**, 184303 (2024).
- [35] X. Wang, J. Bai, J. Wang, Z. Cheng, S. Qian, W. Wang, G. Zhang, Z.-M. Yu, and Y. Yao, Real Topological Phonons in 3D Carbon Allotropes, *Adv. Mater.* **36**, 2407437 (2024).
- [36] Y. Li, S. Qian, and C.-C. Liu, General construction of three-dimensional Z_2 monopole charge nodal line semimetals and prediction of abundant candidate materials, *Phys. Rev. B* **111**, 125101 (2025).
- [37] H. Xue, Z. Y. Chen, Z. Cheng, J. X. Dai, Y. Long, Y. X. Zhao, and B. Zhang, Stiefel-Whitney topological charges in a three-dimensional acoustic nodal-line crystal, *Nat. Commun.* **14**, 4563 (2023).
- [38] X. Xiang, Y.-G. Peng, F. Gao, X. Wu, and P. Wu, Demonstration of Acoustic Higher-Order Topological Stiefel-Whitney Semimetal, *Phys. Rev. Lett.* **132**, 197202 (2024).
- [39] G. Salerno, N. Goldman, and G. Palumbo, Floquet-engineering of nodal rings and nodal spheres and their characterization using the quantum metric, *Phys. Rev. Res.* **2**, 013224 (2020).
- [40] X.-Q. Sun, S.-C. Zhang, and T. c. v. Bzdušek, Conversion rules for weyl points and nodal lines in topological media, *Phys. Rev. Lett.* **121**, 106402 (2018).
- [41] P. M. Lenggenhager, X. Liu, S. S. Tsirkin, T. Neupert, and T. c. v. Bzdušek, From triple-point materials to multiband nodal links, *Phys. Rev. B* **103**, L121101 (2021).
- [42] M. Wu, M. Weng, Z. Chi, Y. Qi, H. Li, Q. Zhao, Y. Meng, and J. Zhou, Observing relative homotopic degeneracy conversions with circuit metamaterials, *Phys. Rev. Lett.* **132**, 016605 (2024).
- [43] A. Bouhon, Q. Wu, R.-J. Slager, H. Weng, O. V. Yazyev, and T. c. v. Bzdušek, Non-Abelian reciprocal braiding of Weyl points and its manifestation in ZrTe, *Nature Physics* **16**, 1137 (2020).
- [44] M. S. Rudner and N. H. Lindner, Band structure engineering and non-equilibrium dynamics in Floquet topological insulators, *Nat. Rev. Phys.* **2**, 229 (2020).
- [45] T. Oka and S. Kitamura, Floquet Engineering of Quantum Materials, *Annu. Rev. Condens. Matter Phys.* **10**, 387 (2019).
- [46] C. Bao, P. Tang, D. Sun, and S. Zhou, Light-induced emergent phenomena in 2D materials and topological materials, *Nat. Rev. Phys.* **4**, 33 (2022).
- [47] Y. H. Wang, H. Steinberg, P. Jarillo-Herrero, and N. Gedik, Observation of Floquet-Bloch States on the Surface of a Topological Insulator, *Science* **342**, 453 (2013).
- [48] F. Mahmood, C.-K. Chan, Z. Alpichshev, D. Gardner, Y. Lee, P. A. Lee, and N. Gedik, Selective scattering between Floquet-Bloch and Volkov states in a topological insulator, *Nat. Phys.* **12**, 306 (2016).
- [49] E. J. Sie, J. W. McIver, Y.-H. Lee, L. Fu, J. Kong, and N. Gedik, Valley-selective optical Stark effect in monolayer WS_2 , *Nat. Mater.* **14**, 290 (2015).
- [50] Y. H. Wang, H. Steinberg, P. Jarillo-Herrero, and N. Gedik, Ultrafast generation of pseudo-magnetic field for valley excitons in WSe_2 monolayers, *Science* **346**, 1205 (2014).
- [51] N. H. Lindner, G. Refael, and V. Galitski, Floquet topological insulator in semiconductor quantum wells, *Nat. Phys.* **7**, 490 (2011).
- [52] P. Titum, N. H. Lindner, and G. Refael, Disorder-induced transitions in resonantly driven Floquet topological insulators, *Phys. Rev. B* **96**, 054207 (2017).
- [53] P. Titum, N. H. Lindner, M. C. Rechtsman, and G. Refael, Disorder-Induced Floquet Topological Insulators, *Phys. Rev. Lett.* **114**, 056801 (2015).
- [54] T. Oka and H. Aoki, Photovoltaic Hall effect in graphene, *Phys. Rev. B* **79**, 081406 (2009).
- [55] T. Kitagawa, T. Oka, A. Brataas, L. Fu, and E. Demler, Transport properties of nonequilibrium systems under the application of light: Photoinduced quantum Hall insulators without Landau levels, *Phys. Rev. B* **84**, 235108 (2011).
- [56] G. Usaj, P. M. Perez-Piskunow, L. E. F. Foa Torres, and C. A. Balseiro, Irradiated graphene as a tunable Floquet topological insulator, *Phys. Rev. B* **90**, 115423 (2014).
- [57] C.-K. Chan, Y.-T. Oh, J. H. Han, and P. A. Lee, Type-II Weyl cone transitions in driven semimetals, *Phys. Rev. B* **94**, 121106 (2016).
- [58] R. Chen, B. Zhou, and D.-H. Xu, Floquet Weyl semimetals in light-irradiated type-II and hybrid line-node semimetals, *Phys. Rev. B* **97**, 155152 (2018).
- [59] Z. Yan and Z. Wang, Floquet multi-Weyl points in crossing-nodal-line semimetals, *Phys. Rev. B* **96**, 041206 (2017).
- [60] T. Deng, B. Zheng, F. Zhan, J. Fan, X. Wu, and R. Wang, Photoinduced Floquet mixed-Weyl semimetallic phase in a carbon allotrope, *Phys. Rev. B* **102**, 201105 (2020).
- [61] H. Hübener, M. A. Sentef, U. D. Giovannini, A. F. Kemper, and A. Rubio, Creating stable Floquet-Weyl semimetals by laser-driving of 3D Dirac materials, *Nat. Commun.* **8**, 13940 (2017).
- [62] H. Liu, J.-T. Sun, C. Cheng, F. Liu, and S. Meng, Photoinduced Nonequilibrium Topological States in Strained Black Phosphorus, *Phys. Rev. Lett.* **120**, 237403 (2018).
- [63] Z. Yan, R. Bi, H. Shen, L. Lu, S.-C. Zhang, and Z. Wang, Nodal-link semimetals, *Phys. Rev. B* **96**, 041103 (2017).

- [64] A. K. Ghosh, G. C. Paul, and A. Saha, Higher order topological insulator via periodic driving, *Phys. Rev. B* **101**, 235403 (2020).
- [65] M. Rodriguez-Vega, A. Kumar, and B. Seradjeh, Higher-order Floquet topological phases with corner and bulk bound states, *Phys. Rev. B* **100**, 085138 (2019).
- [66] B. Huang and W. V. Liu, Floquet Higher-Order Topological Insulators with Anomalous Dynamical Polarization, *Phys. Rev. Lett.* **124**, 216601 (2020).
- [67] W. Zhu, Y. D. Chong, and J. Gong, Symmetry analysis of anomalous Floquet topological phases, *Phys. Rev. B* **104**, L020302 (2021).
- [68] X.-L. Du, R. Chen, R. Wang, and D.-H. Xu, Weyl nodes with higher-order topology in an optically driven nodal-line semimetal, *Phys. Rev. B* **105**, L081102 (2022).
- [69] Z.-M. Wang, R. Wang, J.-H. Sun, T.-Y. Chen, and D.-H. Xu, Floquet weyl semimetal phases in light-irradiated higher-order topological dirac semimetals, *Phys. Rev. B* **107**, L121407 (2023).
- [70] B.-Q. Wang, H. Wu, and J.-H. An, Engineering exotic second-order topological semimetals by periodic driving, *Phys. Rev. B* **104**, 205117 (2021).
- [71] S. Ghosh, K. Saha, and K. Sengupta, Hinge-mode dynamics of periodically driven higher-order weyl semimetals, *Phys. Rev. B* **105**, 224312 (2022).
- [72] K. Taguchi, D.-H. Xu, A. Yamakage, and K. T. Law, Photovoltaic anomalous Hall effect in line-node semimetals, *Phys. Rev. B* **94**, 155206 (2016).
- [73] C.-K. Chan, P. A. Lee, K. S. Burch, J. H. Han, and Y. Ran, When Chiral Photons Meet Chiral Fermions: Photoinduced Anomalous Hall Effects in Weyl Semimetals, *Phys. Rev. Lett.* **116**, 026805 (2016).
- [74] A. Gupta, Floquet dynamics in multi-Weyl semimetals, [arXiv:1703.07271](https://arxiv.org/abs/1703.07271) .
- [75] H. Xu, J. Zhou, and J. Li, Light-Induced Quantum Anomalous Hall Effect on the 2D Surfaces of 3D Topological Insulators, *Adv. Sci.* **8**, 2101508 (2021).
- [76] Z. Ning, B. Zheng, D.-H. Xu, and R. Wang, Photoinduced quantum anomalous hall states in the topological anderson insulator, *Phys. Rev. B* **105**, 035103 (2022).
- [77] Z. Yan and Z. Wang, Tunable Weyl Points in Periodically Driven Nodal Line Semimetals, *Phys. Rev. Lett.* **117**, 087402 (2016).
- [78] A. Menon, D. Chowdhury, and B. Basu, Photoinduced tunable anomalous Hall and Nernst effects in tilted Weyl semimetals using Floquet theory, *Phys. Rev. B* **98**, 205109 (2018).
- [79] T. Nag, A. Menon, and B. Basu, Thermoelectric transport properties of Floquet multi-Weyl semimetals, *Phys. Rev. B* **102**, 014307 (2020).
- [80] A. Castro, U. De Giovannini, S. A. Sato, H. Hübener, and A. Rubio, Floquet engineering the band structure of materials with optimal control theory, *Phys. Rev. Res.* **4**, 033213 (2022).
- [81] S. Higashikawa, M. Nakagawa, and M. Ueda, Floquet chiral magnetic effect, *Phys. Rev. Lett.* **123**, 066403 (2019).
- [82] L. Li, C. H. Lee, and J. Gong, Realistic floquet semimetal with exotic topological linkages between arbitrarily many nodal loops, *Phys. Rev. Lett.* **121**, 036401 (2018).
- [83] J. H. Shirley, Solution of the Schrödinger Equation with a Hamiltonian Periodic in Time, *Phys. Rev.* **138**, B979 (1965).
- [84] H. Sambe, Steady States and Quasienergies of a Quantum-Mechanical System in an Oscillating Field, *Phys. Rev. A* **7**, 2203 (1973).
- [85] L. Li, C. Cui, R.-W. Zhang, Z.-M. Yu, and Y. Yao, Planar Hall plateau in magnetic Weyl semimetals, *Sci. Bull.* **70**, 187 (2025).
- [86] L. Li, J. Cao, C. Cui, Z.-M. Yu, and Y. Yao, Planar Hall effect in topological Weyl and nodal-line semimetals, *Phys. Rev. B* **108**, 085120 (2023).